Effects of Functionalization on Photo-Actuatable Octa(dimethylsiloxy)silsesquioxane-Azobenzene Network Gels and their Substance Loading and Unloading Efficiencies

Cory B. Sims, Ethan T. Chandler, Herenia Espitia Armenta, Nai-hsuan Hu, Joseph C. Furgal*

Department of Chemistry and Center for Photochemical Sciences, Bowling Green State University, Bowling Green, OH 43403, USA

*Correspondence should be addressed to Dr. Joseph C. Furgal: furgalj@bgsu.edu

Abstract

The synthesis, characterization, analysis, and effect on solvent uptake of styrene, alcohol, amino, and perfluoro functionalized silsesquioxane-azobenzene hybrid gels are discussed. 4,4'-diallyloxyazobenzene and octa(dimethylsiloxy)silsesquioxane ($Q_8M_8^H$) gels are generated using hydrosilylation chemistry. These gels were modified through two routes: in-situ and post-synthesis modification, depending on the compatibility of the modifiers. The dynamic gel systems react to visible and UV light to expand and contract, giving them sponge-like properties. The general characteristics of each gel are illustrated through UV-Vis, ATR-FTIR, TGA, NMR, and SEM imaging. Effects on their solvent uptake load and preference for various solvents/pollutants are detailed below, and notable findings include preferences of the styrene material for aromatics, perfluoro for THF, and alcohol for acetone. This is accompanied by a low affinity for water, enabling them to remove organic solvents and particulate from water. We find that selectivity for certain substances can be obtained but at the cost of total absorptivity of the gel systems.

Keywords: Environmental Remediation, Photo-actuatable, Smart-gels, Azobenzene, Silsesquioxane, Spherosilicate

1. Introduction

In recent years, research has led to the understanding that many different pollutants have become integrated into natural waterways and omnipresent within our drinking water, resulting in a need to remediate such contaminants from water in more efficient, reusable manners.[1–3] The use of porous polymers, which can remove or absorb pollutants from aqueous systems, has become a significant research focus for this purpose. The design of responsive, smart gel polymer networks that absorb liquids has benefited several fields and shows potential for use as absorbents or sponges.[4–7]

In biomaterials, gels have been used for long-term dosage delivery,[8] but environmental response has been implemented to degrade gels in the presence of specific molecules like glucose,[9] delivering its contents in response, like insulin or small proteins. Successful degradation has been achieved by using proteins[8,10–12] and polysaccharides[13] as biologically compatible scaffolding. Other designs to specify target interactions with liquids or particles have utilized changes to materials by the addition of binding sites, changes in polarity, or alterations to pH through added functionality.[11,14–18] For use in remediation, the functionalization of materials has proven beneficial for adding selectivity or preference for interactions of gels with specific analytes, waste, and pollutants.[19,20] Integration of poly[[N-isopropylacrylamide-co-4-(3-acryloylthioureido) benzoic acid)0.35][21] and 4-(3-acryloyl-thioureido)-benzoic acid[22] into silica gel enabled targeted

adsorption of phosphoproteins through hydrogen bonding with the phosphate, indicating the incorporation of hydrogen bonding moieties into porous structures allows for interactions with phosphorous containing molecules. Functionalizing silicas with pyridine, thiol, and amine groups has increased the material's adsorption of pharmaceuticals like ibuprofen.[23] Integration of dopamine into silica microspheres has enabled a pH-responsive alteration of the material's hydrophilicity.[15] In contrast, hydrophobicity has been tuned in smart gels by adjusting the material's butyl methacrylate composition ratio.[24] Polarity has been affected by adding azobenzene photo-switches into silica to cause a reversible shift, which intensifies depending on the irradiation time.[16]

Using these azobenzenes (or its derivatives) has another primary purpose: the light-driven actuation of materials.[25–27] This group of molecules was found to have a reversible isomerization caused by absorbance of UV light, exciting the N=N double bond, allowing the molecule to rotate and convert from the stable trans form to the cis. When coupled with the strain of the cis isomer, the use of visible light excites the bond again, allowing it to relax into the trans conformation. The wavelengths necessary for activation in these molecules have been altered by substituting the system's benzene rings. One of the primary goals of this is to make the molecule absorption red-shift, allowing for a trans→cis isomerization with non-harmful visible light for use in biological studies.[27–30] Other research has focused on the integration of these molecules as crosslinkers in different types of materials through the addition of polymerizable substituents like allyloxy.[25,31–33] Kumar and Neckers described the structural changes in disubstituted azobenzene monomers as caused by isomerization of the N=N bond in the photo-excited state to reduce the distance between the 4 and 4' para carbons by roughly 3.5 Å (9Å → 5.5 Å).[34,35] The change in the crosslinker's size is observed across all azobenzene bonds within the network upon irradiation, altering the entire material's characteristics. For these reasons, azobenzenes have been used as crosslinkers in photo-healable networks,[36] optics,[37] thermal energy storage molecules,[38] photo-switchable adhesives,[39] pollutant absorbents,[40] photo-responsive thin films[35], and gels.[41]

The integration of azobenzenes into sponge-like materials provides the potential for hands-free absorbance and release of environmental pollutants. Early attempts at using azobenzenes in "sponge" materials utilized hydrogels that showed moderate actuation (~20%), but these materials required an aqueous environment.[42,43] This reduces the ability of the material to absorb non-aqueous substances and suggests a need for an alternative porous-forming structural component. Silsesquioxanes are widely used precursors in many polymerization processes for silicon-based materials. The Q-type silica cage, which, for simplicity, we will refer to as silsesquioxane ($Q_8M_8^H$, Q_8, octakisdimethylsiloxy-silsesquioxane), has terminal silanes that allow for cross-linking via hydrosilation reactions using a platinum catalyst such as Karstedt's (Figure S1).[44–47] Integration of these silsesquioxanes with azobenzenes has resulted in photo-responsive molecules,[48–52], nanocomposites,[31,53] films,[54] and gels[51,55,56] through the reversible cis-trans conversion. Polymerization of 4,4'-diallyloxy-azobene with Q_8 has resulted in photo-responsive sponges, demonstrating a reversible actuation of (~18%), comparable to the hydrogels, while in non-aqueous solvents.[56] This shows the potential of these materials as pollutant sponges and provides an avenue for improved selectivity.

The synthesis, analysis, and effect on solvent uptake of functionalized silsesquioxane-azobenzene hybrid gels are discussed in comparison to the original material below. 4,4'-diallyloxy-azobenzene and octa(dimethylsiloxy)silsesquioxane ($Q_8M_8^H$) gels are generated using hydrosilylation chemistry and Karstedt's catalyst, where bond formation occurs between the

alkene of the allyloxy group and the terminal silanes of the silsesquioxane (Figure 1).[56] The actuation of each cross linker causes the gel systems to be dynamic, reacting to UV and visible light to contract and expand, giving them sponge-like properties (Figure 2). These gels were modified with various functional groups through two routes: in-situ and post-synthesis-modification, where the functional alkene reacts with unbound silanes within the cage network utilizing residual catalyst. Previous research demonstrated the ability to add allyl groups, such as allyl alcohol, to $Q_8M_8^H$ using this catalyst without quenching the catalyst.[57]
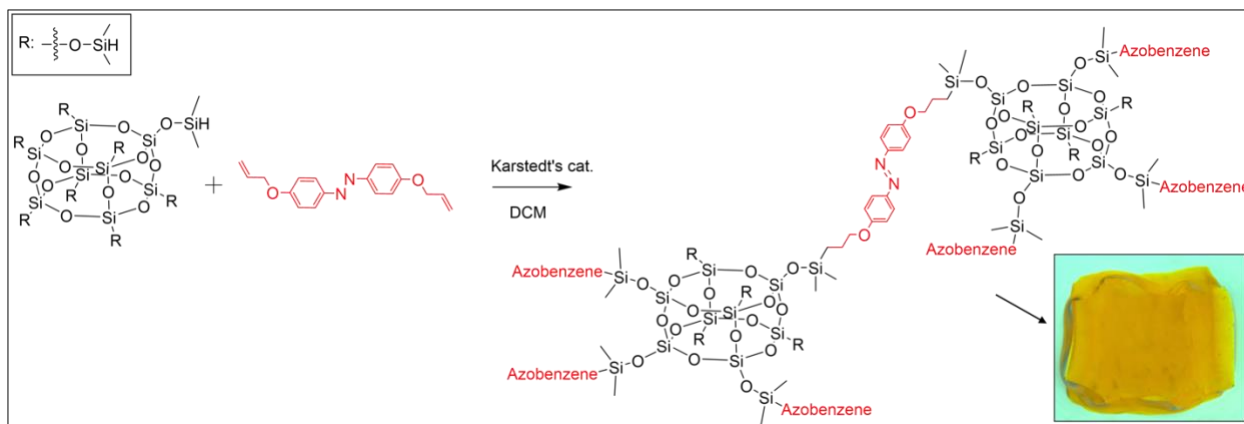

Figure 1. Reaction of octa(dimethylsiloxy)silsesquioxane ($Q_8M_8^H$) and 4,4'-diallyloxyazobenzene (azo, red) to form the cross-linked network in dichloromethane (DCM).
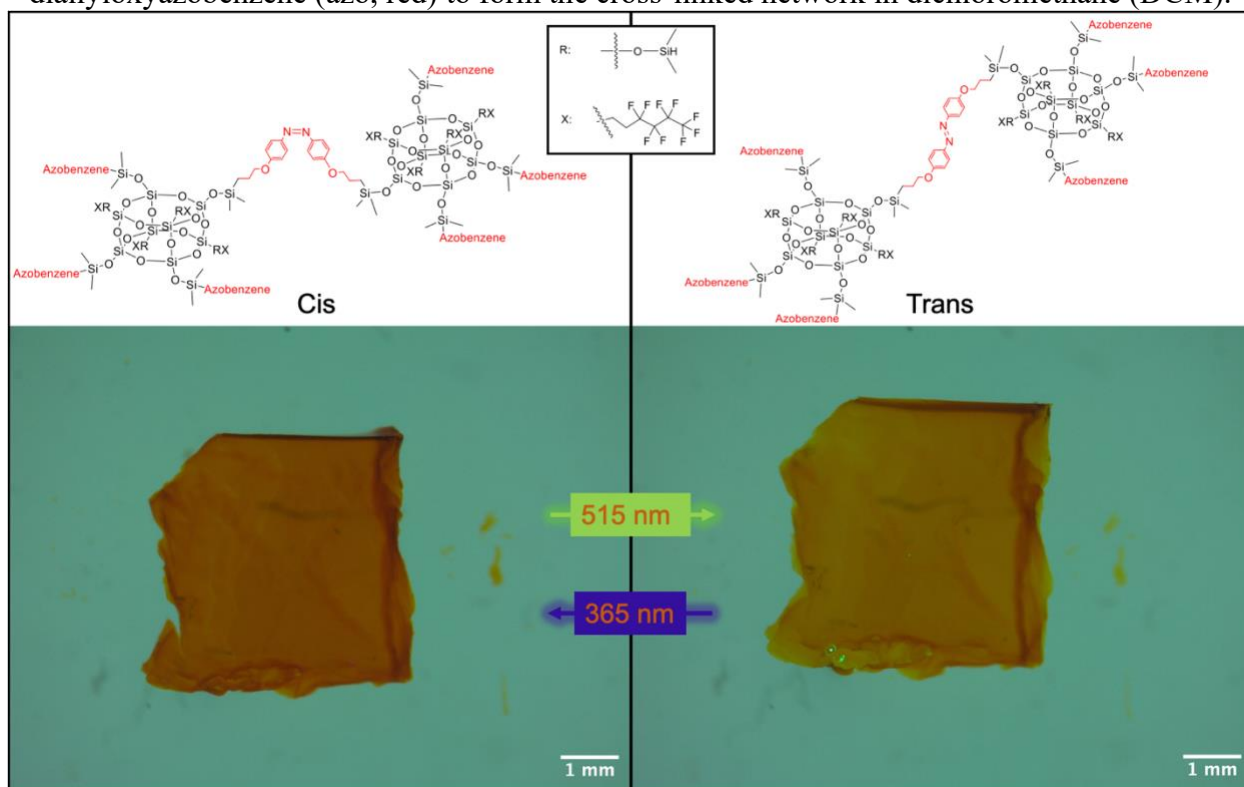

Figure 2. Structural and physiological changes observed in functionalized azobenzene cross-linked silsesquioxane gels when exposed to UV (365 nm) and green visible (515 nm) light.

3

The analysis of solvent swellability described herein provides insight into the potential use of these materials as hands-off sponges, which can selectively absorb pollutants from water or other liquid environments. These materials can be swollen from a dry state or using green (515 nm) light and wrung out with UV, reducing the need for direct contact. The effects on their solvent uptake load and preference for various environmental pollutants are detailed below, and general characteristics are illustrated through FTIR, TGA, and optical/SEM imaging.

2. Experimental Methods

2.1. Materials

All materials and items were purchased from vendors or donated and used as received unless described here within. Dichloromethane (DCM) and acetone were purchased from EMD Chemicals. Toluene and tetrahydrofuran (THF) were obtained from Supelco. Hexafluorobenzene (99.0%), styrene (>99.0%), and 3,3,4,4,5,5,6,6,6-nonafluoro-1-hexene (>98.0%) were all obtained from TCI America. Allylamine (98%) was purchased from Sigma-Aldrich, and allyl alcohol (98+%) through Thermo Fisher Scientific. Karstedt's catalyst (platinum-divinyltetramethyldisiloxane complex, 2% Pt in xylene) was obtained from Gelest, Inc. 1,1,1-trichlorotrifluoroethane (CFC) was bought from Synquest Labs Inc. 9-fluorenone (98+%) was purchased from Alfa Aesar. Both gasoline (regular unleaded) and diesel were obtained from Marathon. Reverse osmosis purified water was used in all testing. Norm-Ject®-F Leur Solo 1mL syringes were used with hypodermic needles (18Gx 1 ½" Luer-Lock, Air-Tite Products Co., Inc.) for the injection of solutions. The 365 nm lamp was purchased from ThorLabs (COP1-A Olympus - M365LP1-C1 15.0V Lamp), and Lumenshooter made the 515 nm flashlight. Octakis(dimethylsiloxy)silsesquioxane ($Q_8M_8^H$) were provided by Mayaterials Inc., Ann Arbor, MI. 4,4'-diallyloxy-azobenzene synthesized via method by Hu and Furgal.[56]

2.2. Gel Preparation and Solvent Exchange

2.2.1 Preparation of the 1:2 Azo-octa(dimethylsiloxy)silsesquioxane ($Q_8M_8^H$/Azo) polymers

The formation of the 1:2 mol ratio $Q_8M_8^H$/Azo gels was modified from the methods used by Hu and Furgal.[56] In a 20 mL vial, 0.192 g (0.2 mmol) $Q_8M_8^H$ and 0.13 g (0.4 mmol) 4,4'-diallyloxy-azobenzene were added together and dissolved in 2 mL DCM. In a separate vial, 1 mL of DCM was mixed with 1 drop (0.0007 mmol Pt) of Kartsedt's catalyst and then added to the other solution. The mixture was warmed to 36 °C to initiate polymerization, and then 2 mL of DCM was added to the vial. The material underwent solvent exchange to remove impurities before cutting and analysis.

2.2.2 Preparation of the 1:2:4 Azo-octa(dimethylsiloxy)silsesquioxane ($Q_8M_8^H$/Azo/Modification) polymers – prefunctionalized

In a 20 mL vial, 0.192 g (0.2 mmol) $Q_8M_8^H$, 0.13 g (0.4 mmol) of 4,4'-diallyloxy-azobenzene, and styrene/3,3,4,4,5,5,6,6,6-nonafluoro-1-hexene (0.8 mmol – 0.090 mL/0.140 mL) were added together and mixed in 2 mL DCM. In a separate vial, 1 mL of DCM was mixed with 1 drop (0.0007 mmol Pt) of Kartsedt's catalyst and then added to the other solution. The mixture was warmed to 36 °C to initiate polymerization, and then 2 mL of DCM was added to the vial

(Figure 4). The material underwent solvent exchange to remove impurities before cutting and analysis.

2.2.3. Preparation of the 1:2:4 Azo-octa(dimethylsiloxy)silsesquioxane ($Q_8M_8^H$/Azo/Modification) polymers – postfunctionalized

In a 20 mL vial, 0.192 g (0.2 mmol) $Q_8M_8^H$ and 0.13 g (0.4 mmol) were added together and dissolved in 2 mL DCM. In a separate vial, 1 mL of DCM was mixed with 1 drop (0.0007 mmol Pt) of Karstedt's catalyst and then added to the other solution. The mixture was warmed to 36 °C to initiate polymerization, and then 2 mL of DCM was added to the vial. After 15 minutes, a 1 mL solution of DCM and allyl alcohol/allyl amine (0.8 mmol – 0.055 mL/0.060 mL) were slowly injected into the middle of the gel with a syringe (1 mL, 20 g needle). After 24 hours, the material underwent solvent exchange to remove impurities before cutting and analysis. Synthesis is shown in Figure 3.
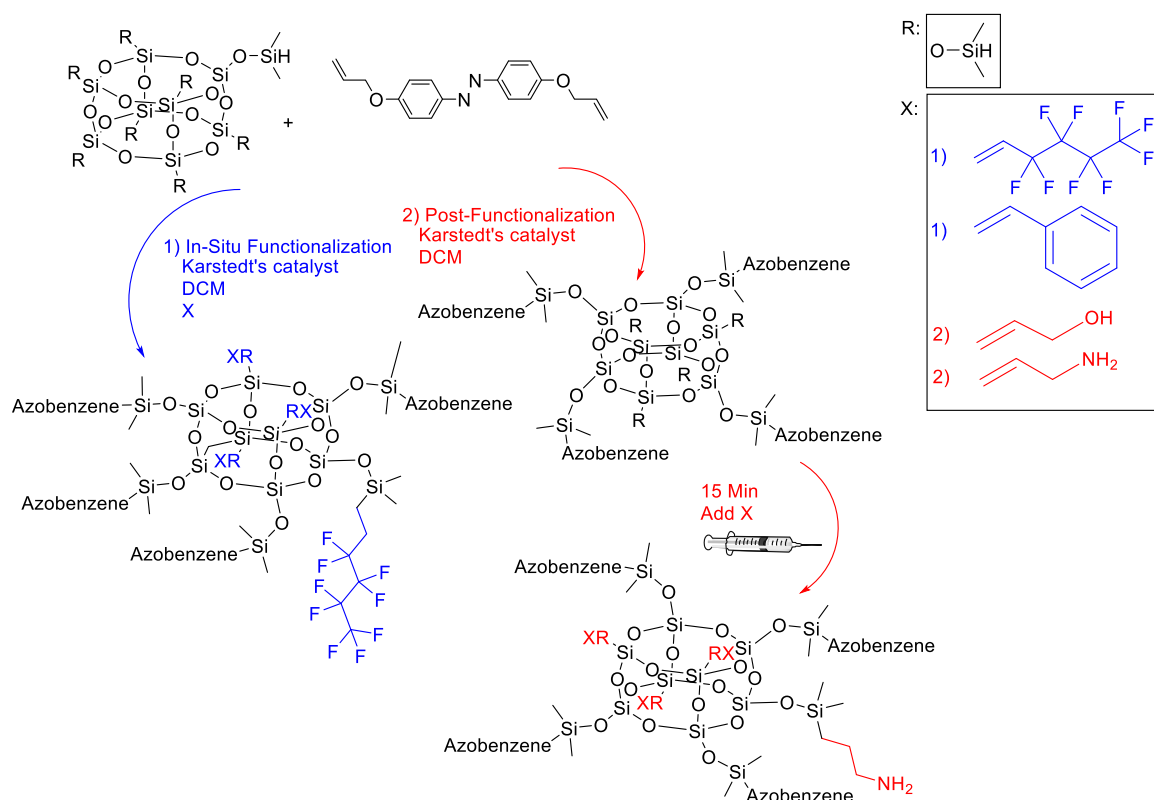

Figure 3. Formation of functionalized gels using in-situ (blue) and post (red) functionalization methods.

2.2.4. Solvent Exchange and Analysis

Gels underwent an exchange process in between analyses. Samples in vials had existing solvent decanted and new solvent added (~90%) to promote diffusion of unutilized reagents and an exchange of solvents. Samples were allowed to rest in ambient conditions with the new solvent for 2 hours before the process was repeated for a total of 3 replacements. This process was performed 24 hours after the initial gel synthesis and after each solvent study to remove impurities and ensure solvent replacement through diffusion. Samples were analyzed by light microscopy (section 2.3) during actuation. Initial images were obtained, then samples were irradiated for 3

cycles of 365 nm (UV – 30 minutes) and 515 nm (Green – 30 minutes), with images taken at each step. If a gel degraded, a new sample was imaged in DCM and exchanged into the solvent of interest, and the calculations were based on the new solvent by percentage.

2.2.5. Solvent Preferability Analysis

Solvent miscibility and preference effects were studied using water, DCM, and THF solutions. First, a sample of styrene functionalized gel was exchanged into DCM. The sample was then placed on a glass petri dish and encapsulated in water by a pasture pipette. UV light was used to irradiate the sample for 16 minutes while recording the process by light microscopy. Second, a 1 M 9-fluorenone solution of 1:1 (1 mL water – 1 mL THF) was made, and after gentle mixing, 2 drops of the solution were added to a partially dried styrene functionalized gel that had been stored in water. The solution was exposed to 515 nm light to facilitate absorption, and the process was recorded using light microscopy. Still frame images were generated from each video to demonstrate the material's solvent selectability.

2.3. Light Microscopy and Surface Area

A Zeiss Stemi 2000-C light microscope (Carl Zeiss Meditec Inc., Dublin, CA, USA) equipped with an AxioCam ERc5s camera at 0.65 x magnification was used to capture images. The perimeter of the gels and background was highlighted using the Magic Wand Tool in Adobe Photoshop (V. 25.1.0), and the difference between the selected pixels and the entire picture was recorded (Formula 1). These values were used to compute the variations in different solvents with respect to the sample size in the beginning. *Note: Using a consistent setting on the microscope produces images with identical pixel counts (307,200 pixels).*

Formula 1. Equation used to generate the surface area in pixels for comparative analysis.

$$Surface\ Area = Total\ Image\ Pixels - Highlighted\ Background\ Pixels$$

2.4. Dry-Swelling Analysis

The DCM swollen gels were allowed to dry out completely over 24 hours in ambient conditions through evaporation prior to imaging. Then, the gels were exposed to DCM and allowed to reswell, and images were taken. The microscope images were used to assess the approximate change in surface area by percentage of the dried sample.

2.5. UV-Vis Spectroscopy

Using an Agilent (Santa Clara, CA, USA) Cary 60 UV/Vis, a series of absorbance spectra were obtained. Dichloromethane swollen gel systems were put in a quartz cuvette (reduced volume 1 cm x 1 cm with 2 mm sample path length) containing DCM. Every seven seconds, until the actuation stopped, a series of scans were taken between 200 and 800 nm. Using 365 nm or 515 nm light, an overlay of the absorbance vs. wavelength was plotted during the length of the conformational shift using Microsoft Excel.

2.6. Fourier Transform Infrared Spectroscopy – Attenuated Total Reflection (ATR-FTIR)

Spectra was obtained using OMNIC Spectra (Thermo Scientific, Waltham, MA, USA, 2017) on a Thermo Scientific ATR-FTIR (Nicolet iS5 Fourier Transform Infrared Spectrometer iD7 Attenuated Total Reflection, SN: ASB1817610). ATR methods were used, and solid samples were placed directly on a ZnSe crystal. All samples had 16 scans from 4000 to 400 cm−1 with 0.121 cm−1 data spacing. Post-analysis was performed using Microsoft Excel (Version 2305 Build 16.0.16501.20074) 64-bit.

2.7. Thermal Gravimetric Analysis (TGA)

Thermal gravimetric analysis was conducted using a Hitachi STA7200 Thermal Analysis System and NEXTA. Before examination, materials were dried in a vacuum oven (50°C for 48 hours). 5-20 mg samples were placed in a ceramic crucible and heated at 10 °C per minute from 25 to 1000 °C, with an airflow of 200 mL/min. Data was extracted and graphed for analysis in Microsoft Excel.

2.8. MAS SS ^{29}Si NMR

Magic Angle Spinning Solid-state ^{29}Si NMR and ^{13}C were collected using a Bruker 600MHz Avance IIIHD DNP spectrometer (Bruker, Inc., Billerica, MA, USA). Ground samples were packed into 3.2 mm zirconium rotors, spun at 10kHz MAS frequency, and heated to ~300K. A 3.2 mm HXY-DNP probe was used to collect all data. ^{29}Si utilized H-Si cross polarization experiments (145 to -255 ppm, 256 scans, and 7-second decay period). ^{13}C analysis utilized H-C cross polarization with a spectral window of 296 to -97 ppm. All spectra were generated using MestReNova (v15.0.1-35756) with a Bernstein Polynomial baseline correction. ^{29}Si NMR data were used to approximate functionalization percentages based on relative peak heights of the Si-H and Si-C shifts.

Original gel – ^{29}Si NMR (δ ppm): δ 12.11, -2.89, -109.78; ^{13}C NMR (151 MHz, δ ppm): δ 229.65, 215.60, 193.02, 183.18, 163.38, 149.28, 126.74, 116.91, 97.14, 83.04, 72.36, 60.38, 50.88, 32.06, 25.43, 18.88, 15.99, 11.55, 2.20.

Styrene gel – ^{29}Si NMR (δ ppm): δ 11.52, 9.16, -3.04, -109.93; ^{13}C NMR (151 MHz, δ ppm): δ 229.75, 215.60, 195.88, 180.77, 163.45, 149.22, 130.26, 116.94, 72.43, 65.87, 33.11, 31.48, 27.79, 25.37, 22.02, 16.46, 14.26, 11.75, 2.01, 0.47, -0.34.

Nonafluoro gel – ^{29}Si NMR (δ ppm): δ 12.16, 6.50, -2.94, -110.08; ^{13}C NMR (151 MHz, δ ppm): δ 229.65, 215.58, 192.97, 183.24, 163.46, 149.27, 126.71, 116.88, 97.21, 72.34, 60.46, 50.47, 31.92, 25.38, (18.88), 15.88, 11.48, 9.27, 1.59.

Amine gel – ^{29}Si NMR (δ ppm): δ 11.08, -3.19, -19.58, -110.22; ^{13}C NMR (151 MHz, δ ppm): δ 229.75, 215.47, 193.09, 183.06, 163.49, 149.28, 132.18, 126.76, 116.99, 97.27, 82.93, 72.60, 47.00, 29.72, 25.48, 16.46, 11.72, 2.39.

Alcohol gel: ^{29}Si NMR (δ ppm): δ 12.11, -109.73; ^{13}C NMR (151 MHz, δ ppm): δ 229.84, 215.53, 193.18, 183.28, 163.54, 149.29, 126.87, 117.12, 97.28, 82.89, 72.63, 67.02, 28.54, 25.38, 15.98, 2.04.

2.9. Scanning Electron Microscopy (SEM)

Dried samples were mounted to the sample spaceman with a carbon adhesive strip revealing exterior and interior surfaces occurring from fracturing when drying. A conductive layer was applied using a Hummer VI-A Sputter Coater (gold/palladium mix). Mounted samples were placed inside the instrument, and images were obtained using a Hitachi S-2700 Scanning Electron Microscope with a lanthanum hexaboride source (Hitachi, Tokyo, Japan). Images were obtained using 70× magnification with working distances of 13-14, 15 kV, and an aperture of 4.

3. Results and Discussion

Octakisdimethylsiloxy-spherosilicate ($Q_8M_8^H$, Q-silsesquioxane) – 4,4'-diallyloxy-azobenzene (azo) photo-responsive gels were synthesized according to the methods described in Section 3 using hydrosilylation in DCM, and the addition of the functional group in-situ or post-polymerization. The original gel system was designed to be photo-actuatable, and the functionalized variants retain their photo-responsive nature at varying efficiency in the presence of different solvents. The mol ratio of 1:2 $Q_8M_8^H$-Azo was used as its previous work showed its actuation was the largest compared to other formulations.[56] Functionalized gels were formed with a mol ratio of 1:2:4 ($Q_8M_8^H$:azo:functional group) to show the effect of the moiety on solvent absorption while reducing the impact on actuation efficiency. With some variation from the random polymerization, using this composition of components, each cage within the gel is expected to, on average, have no unbound corners, with half of the corners bound to an azobenzene, and half to the functional groups base on stoichiometry. Styrene, 3,3,4,4,5,5,6,6,6-nonafluoro-1-hexene (nonafluoro, fluoro), allylamine (amine), and allyl alcohol (alcohol) were chosen due to their difference in potential solvent interactions (Figure 4). Functional group reactivity with the catalyst (platinum) was considered in the choice of incorporation method, where alcohol and amine groups were added post-gelation. Interaction of the functionality with the catalyst may still occur, as discussed herein, but this preparation method aimed to reduce these instances. Gels were characterized by UV-Vis, ATR-FTIR (attenuated total reflection-Fourier-transform infrared spectroscopy), TGA (thermogravimetric analysis), ^{29}Si SS NMR (Solid State Nuclear Magnetic Resonance) and SEM (scanning electron microscopy) Materials were analyzed by swelling and actuation in different solvents to observe the effects of functionalization. A comparative analysis is provided for insight into the structural, thermal, and geomorphic properties of the polymerized materials with differing functionalities to the original, unmodified $Q_8M_8^H$-azo gel referred to herein as the "original gel".
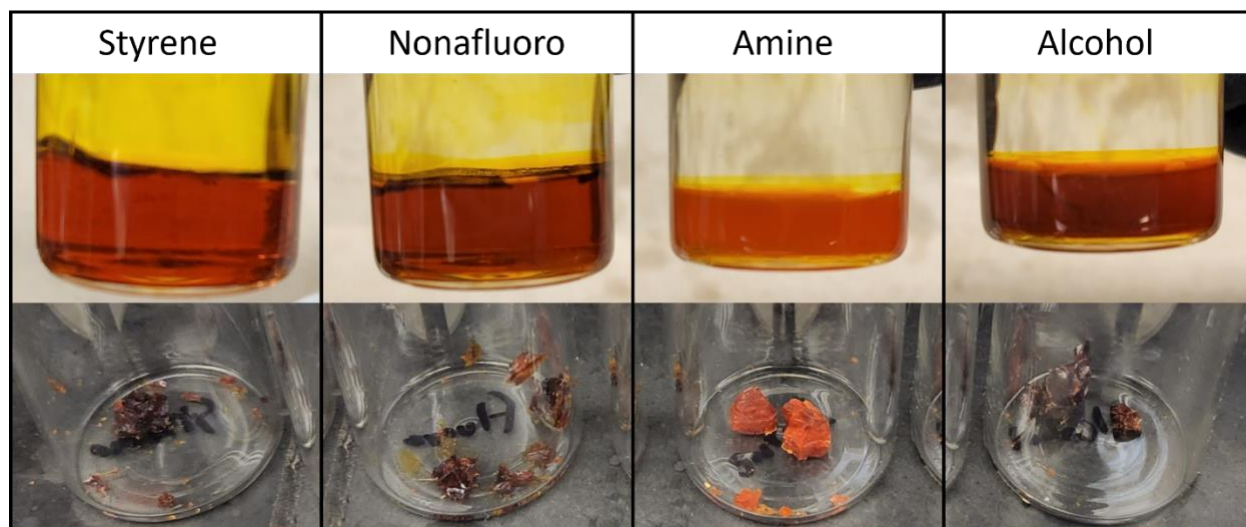
Figure 4. Images (20 mL scintillation vials) of the functionalized gels post-reaction (top) and after solvent exchange and drying (bottom). Styrene and nonafluoro utilized the in-situ method, while the amine and alcohol gel were post-functionalized. Each shows a visible difference in color, texture, and firmness.

3.1. Material Characterization

UV-Vis analysis of the 4,4'-diallyloxyazobenzene gel and each of the functionalized materials shows effects of the functionalization on the photo-actuation of the material. Conversion of the original gel from trans to cis occurs within 175 seconds under UV irradiation where the absorption at 360 nm diminishing over time while the bands at 260 and 460 nm increase. The reverse transformation takes 350 seconds with 515 nm light to completely return to the original state showing the opposite shifts in absorbances and maintaining the isosbestic points of 325 and 430 nm (Figure S2). The styrene gel exhibits a distinct change, where there is no observed isosbestic point, and a reduction in absorbance at 365 nm under UV (105 sec) and increase with green light (560 sec). This is believed to occur due to competitive absorption of the aromatic groups within the material (Figure S3). Both the nonafluoro and amine gels have similar absorption bands and transitions to the original materials with an increase in the intensity of the 265 nm peak (Figures 5 and S4). Despite the similarities, the speed of actuation does change compared to the original gel where the amine converts from trans to cis in 112 seconds and cis to trans over 175 seconds, while the nonafluoro gel has a faster trans to cis conversion (105 sec) but slower cis to trans (245 sec). The alcohol functionalized gel acts more similarly to the styrene material, where there is a reduction in absorption at 365 nm when exposed to UV (112 sec) and an increase under green light (420 sec) with no isosbestic point (Figure S5). This may be an indication of competitive absorption occurring from functionalization at the hydroxy end, leaving the allyl group in the exterior of the material. An alternative explanation would be a reduction in the amount of 4,4'-allyloxyazobenzene bound to each cage due to excessive attachment by the functional group. Overall, each material exhibits some absorption at 365 nm, despite the differences in intensities and other peaks observed.
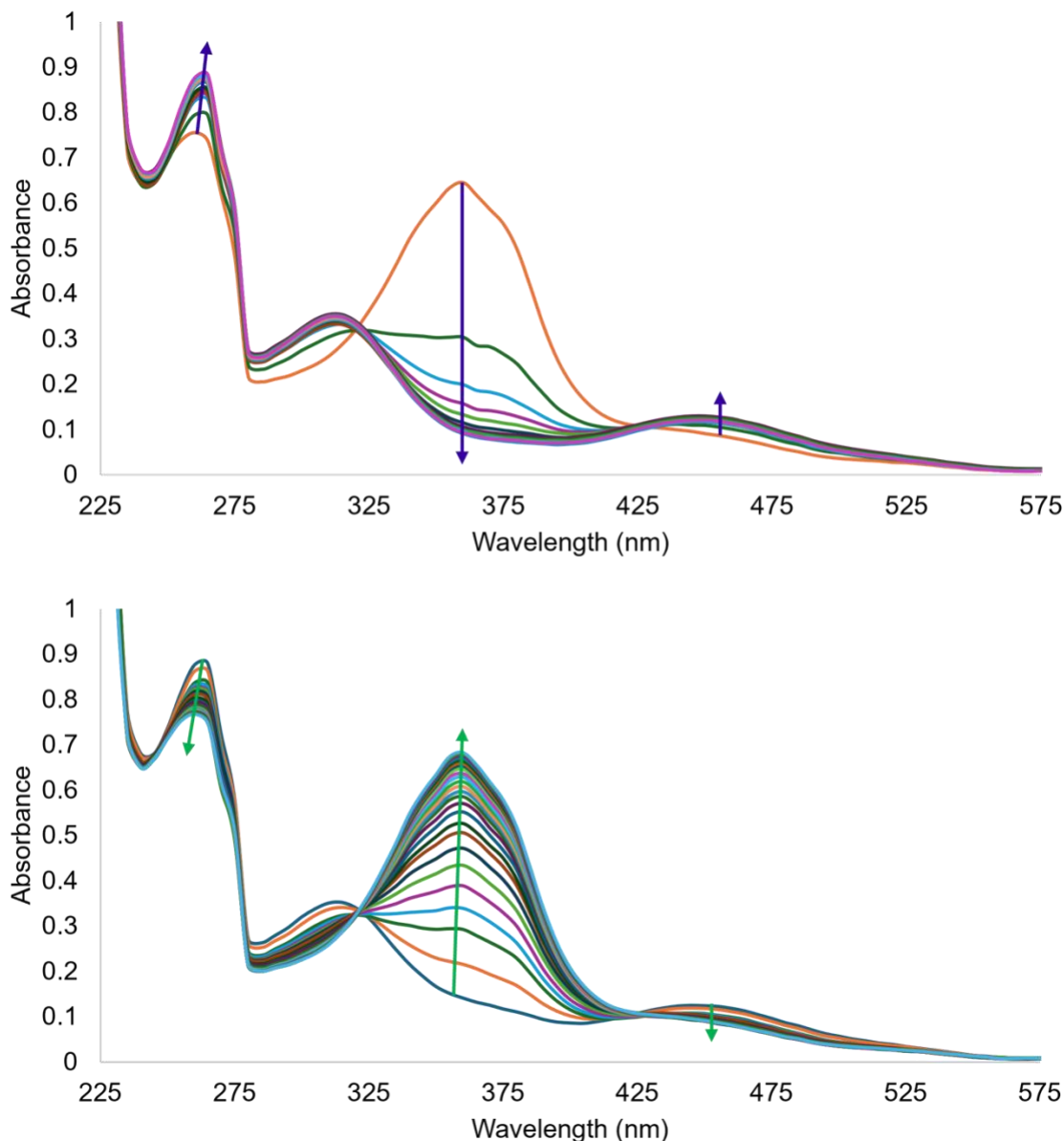
Figure 5. UV-Vis Spectra of the 1-2 $Q_8M_8^H$ – 4,4'-allyloxyazobenzene nonafluoro functional gel. Trans to Cis transition of the azo-crosslinker occurring over 105 seconds of 365nm UV light exposure is shown on top. Conversion from the cis form to the trans happens within 245 seconds of exposure to a 515nm light (bottom). The direction of each transition is shown with arrows.

ATR-FTIR was performed on dried-out samples of each functionalized gel and compared to the original material (Figure S6). Each material shows the presence of the Si-O-Si (1130-1000 cm^{-1}), Si-H (2280-2080, 950-800 cm^{-1}), and Si-CH$_3$ (~2960, ~2870, ~1380, and 1275-1245 cm^{-1}) peaks from the Q_8-silsesquioxanes but distinct resonances also show their functional groups. These peaks may be present in each sample as the polymers are formed randomly, so not every cage unit will have full functionality or crosslinking. The spectra of the styrene functionalized gel shows high conversion of the Si-H groups compared to the original material by the reduction in the peaks

at 2139 and 895 cm^{-1}. This is easily observed when the spectra are adjusted to show similar peak heights for the Si-CH$_3$ peaks, showing a similar reduction of the Si-H group in all functionalized gels. The presence of the styrene's aromatic ring is observed in the unsaturated region at 3078, 3060, and 3024 cm^{-1}. In the nonafluoro material, the N=N peak of the azobenzene crosslinker is more visible in the 2020 cm^{-1} region; however, this functional group's resonances, such as C-F (1100-1000 cm^{-1}), overlap with the Si-O-Si section and little more inferences can be made. The amine gel was synthesized post-gelation due to its hindrance to the polymerization process. Spectra of the amine material does not show any notable peaks, but there is noise present in both the primary amine (3500 cm^{-1}) and aliphatic amine (~1650-1540 cm^{-1}) regions; the latter is also broadened. In the alcohol-modified gel, the presence of the OH group is clearly observable by the broad peak around 3400 cm^{-1}. While the results of the FTIR analysis supports the attachment of each functional group by both in-situ and post-gelation methods inferring attachment efficiency is best left for the clearer spectral comparisons obtained by ^{29}Si NMR.

Thermal gravimetric analysis was performed on each of the original and functionalized gels. Each modified gel exhibits a difference in the decomposition temperatures at 5% weight loss ($T_{d5\%}$), indicating that adding functionalization alters the thermal stability of the materials, except for nonafluoro (Figure S7). The addition of styrene reduces the stability from 396 °C in the original gel to 375 °C due to the higher content of hydrocarbons, and attachment of this functionality changed the observed ceramic yield (CY) by 18.0% (Table S1) suggesting high functionalization. Gels containing nonafluoro did not alter the $T_{d5\%}$ from the original material; however, as described above, there is a notable reduction in Si-H groups observed in the FTIR. The shape of the TGA plot is also notably different, with a steadier degradation slope, and a 9.8% observed change in the CY suggests a lower attachment efficiency. Reduction in functionalization by nonafluoro is most likely due to the repellent nature of perfluoroalkanes, but this still affects the solvent preference.

Since the amine and alcohol gels were formed prior to functionalization, neither group can reduce the amount of azobenzene bound to the cage like styrene, suggesting the difference in CY occurs strictly from the functional group, whereas the in-situ functionalized gels may be affected in crosslinking. The addition of the amine side group resulted in the only increase in thermal stability, with a $T_{d5\%}$ of 425 °C (+29 °C). The ceramic yield of the amine gel was 54.5%, only 3.3% lower than the original material, suggesting a reduced attachment efficiency. This is potentially due to interactions with the catalyst as attempting to form the gel through in-situ methods failed, with no gel formation after 24 hours. Lack of polymerization was attributed to quenching of the catalyst by the amine in these trials, and the reduced attachment rate via post-functionalization could result from similar issues. Despite this, there is still a noteworthy alteration in the final materials' solvent preferences and thermal stability. The alcohol gels show the lowest thermal stability with a significant mass reduction beginning at 290 °C suggesting there was either poor attachment of the allyl alcohol or the degradation products are more volatile. The ceramic yield suggests that the material was adequately functionalized, with a difference in CY of 12.8%. As previously mentioned, other researchers have shown that allyl alcohol preferentially reacts at the C, not O, terminal end when attaching it to Q$_8$M$_8^H$ with Karstedt's catalyst,[57] suggesting the material should have retained the free hydroxy terminations, unlike allyl amine. This is further supported by the gel's preference for acetone, a more polar solvent, where C terminations would reduce this preference.
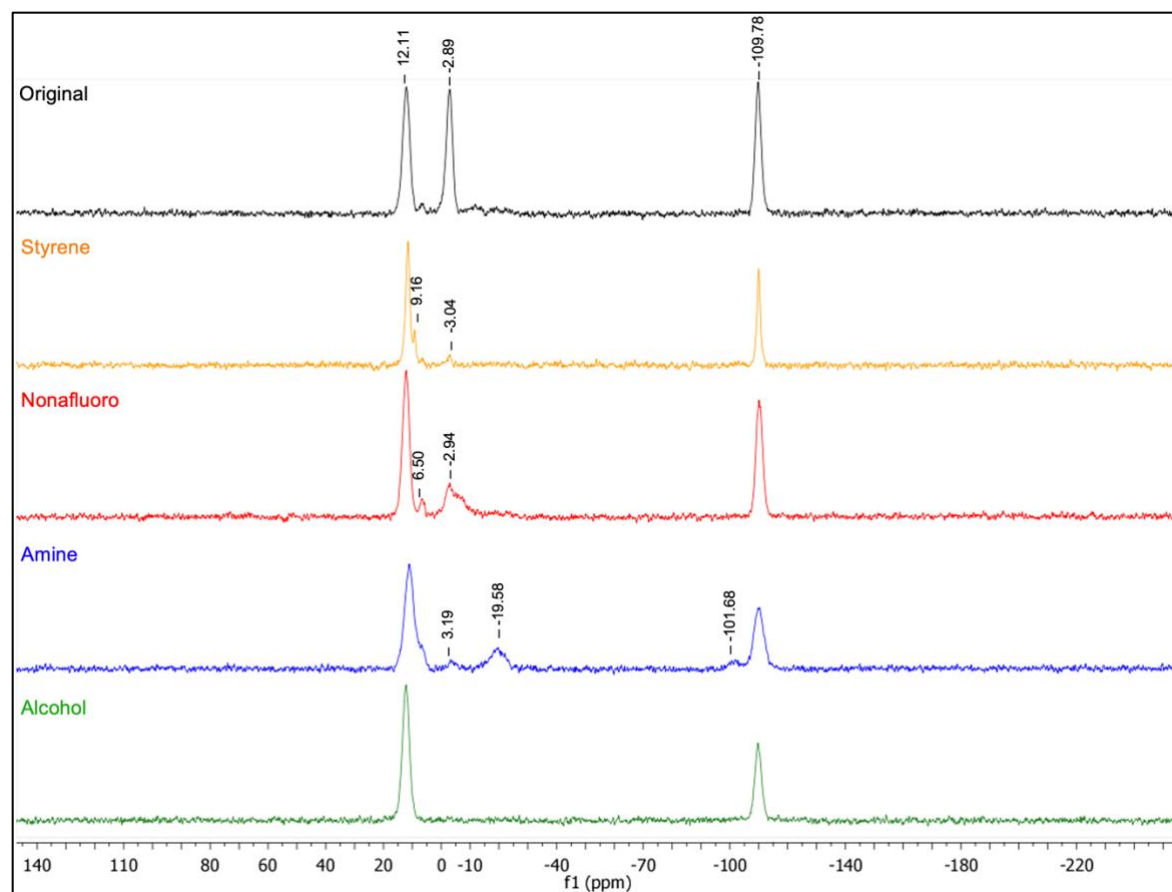
Figure 6. Stacked spectra of the ^{29}Si NMR spectra of each gel.

NMR analysis shows differences in each materials constitution when both silicon and carbon are investigated. ^{29}Si NMR shows the differences between the silicons present in the material, which can show specific changes correlating to the cage and its corners (Figure 6). The original material exhibits peaks with nearly equal intensities at 12.11 [-OSi(Me)$_2$CH$_2$R, allyoxyazobenzene bonding], -2.89 [-OSi(Me)$_2$H, Q-cage corner], and -109.78 ppm [Q$_4$-type, Si(OSi)$_4$, cage structure][58]. This supports that the 1:2 (Q-cage:azo) ratio results in four unbound and four crosslinked corners. In each of the functionalized materials there is a decrease in peak intensity for the peaks around -2.89 and 109.78 ppm, showing a reduction of the Si-H termination. Beyond this, the changes are unique to each material, with several having a shoulder at ~10 ppm indicating attachment of a similar -OSi(Me)$_2$CH$_2$R structure, shifted by the distinct functional group. In the styrene material, there is an additional peak at 9.16 (similar to PhCH$_2$SiCl$_3$ peaks which appear at 7.2 ppm)[59] and -3.04 (Q-cage corner) which suggests that not all of the corners were functionalized, but the majority of this material was (~90+%, peak height estimation). For the nonafluoro gel, there is a peak at -6.50 ppm which we attribute to the -OSi(Me)$_2$CH$_2$R structure with slight shielding occurring from the fluorocarbon chain. This is combined with a larger peak at -2.94 (cage corner), suggesting that the material is lesser functionalized, and based on approximate peak heights may have reached an attachment of ~60+%. In the amine spectra, the shoulder is noticeable around 10 ppm, however it is not clearly defined. There is a peak near -19 ppm suggesting the -OSiMe$_2$R peak shifts upfield due to the propylamine group. This is accompanied by a peak at -101 ppm which is typical of silanol/hydroxy terminated siloxane which

12

may indicate corners which reacted with the nitrogen instead of the allyl end.[59] This is the only material which exhibits this slightly deshielded cage structure, and was the most likely to react at the functional end of the reactive group; however the majority of the Si-H group was reduced (-3.19 ppm), and the amine attachment is the primary unique peak observed, suggesting ~65+% attachment. The alcohol gel shows a full functionalization where the allyl alcohol reacts to form a hydroxypropyl termination, which would show a similar shift to the original cage formed from allyloxy terminated azobenzene; however, there is no presence of the -OSiMe$_2$H peak ~-3ppm. The findings of the ^{29}Si NMR study supports the findings of the FTIR and TGA analysis, which suggested near full functionalization of the styrene and alcohol gels, while the nonafluoro and amine did not react as efficiently.

^{13}C NMR spectra revealed minor differences among the carbons present in each gel sample (Figure S8). Using the H-C cross polarization experiment, there are notable spinning sidebands at 10 kHz over 180 ppm and at 97, 82, 60, and 50 ppm. This was found to be the spinning speed with the least overlap to the shifts of the materials. Across all materials there are some common peaks: For the styrene gel, there is a shift in the peak near 130 ppm (from 126 ppm) which is due to the para carbon of the styrene which lies in the same region as other aromatic carbons on both the styrene and azobenzene. Other variances are seen in shifts from 50-0 ppm due to the reduction in Si-H groups and the presence of the -SiCH$_2$CH$_2$Ar carbons in the functional group. The primary difference between the original and the nonafluoro functionalized gels when viewed by ^{13}C NMR is the presence of an additional peak around 9 ppm which we attribute to the -SiCH$_2$CH$_2$CF$_2$- carbons in the functional group. This peak is at low intensity, suggesting, along with the other characterization methods, that the nonafluoro functional group bound with lower than desired efficiency. There are few differences in the shifts observed in the amine material spectra. The peaks observed at 47, 29, and 16 ppm reflect the propyl formed when the allyl amine binds to the material. This suggests that the primary form of attachment with the amine is through the allyl end. Similar to the amine, the primary differences seen in the alcohol functionalized gel are the shifts at 67 and 28 ppm which occur from the exterior two carbons in the hydroxy propyl chain (-SiCH$_2$CH$_2$CH$_2$OH). Additionally, a lack of the shift at 11 ppm present in every other material may complement the ^{29}Si NMR, indicating the complete functionalization of the material.

When viewed by microscopy, the functionalized gels show some distinct features (Figure S9). Styrene functionalized gels shows smooth ridges with little evidence of strain during formation or shrinking. The nonafluoro gel shows striations across the surface, depressions on the edges, and pore-like structure fractures likely due to incompatibilities between fluorocarbon and the gel material. The amine and alcohol both have smooth surfaces and formed jagged edges where the material was split. Unlike with the original material, there was little observable indication of pores on the surface or interior of the materials.[56] This suggests the functional groups fill the materials' interstitial space, supported by the reduction in solvent uptake.

3.2. Gel Swelling

All gels were inspected for the change in surface area when dried samples were swollen in DCM (Figure 7). The functionalized gels each exhibited distinct firmness in all samples, reducing the ability to produce clean, square cuts, even when using a square punch. To ensure the analysis was accurate, each image was analyzed using an AI-assisted selection tool, and the surface area was measured by pixels since each image was taken with the same microscope settings and the

images contained an identical pixel count and dimensions. This method of analysis considers the X and Y axis changes of the samples for analysis, and a percentage of swelling was calculated by dividing the swollen area by the dry sample.

The original material had a surface area change of 413%, and the functionalized gels decreased in efficiency, starting with styrene (283%), then allyl alcohol (275%), nonafluoro (196%), and lastly, the allyl amine (153%). Each change in area was then compared to the original system as the most efficient in absorption and expansion (Table 1). These measurements were used to generate the graph in Figure S10 and to calculate the relative efficiencies between the original material and modified species. Note that a decrease in swelling was expected in the functionalized versus the original gels due to space-filling through the functionalization of open sites and space within the material.
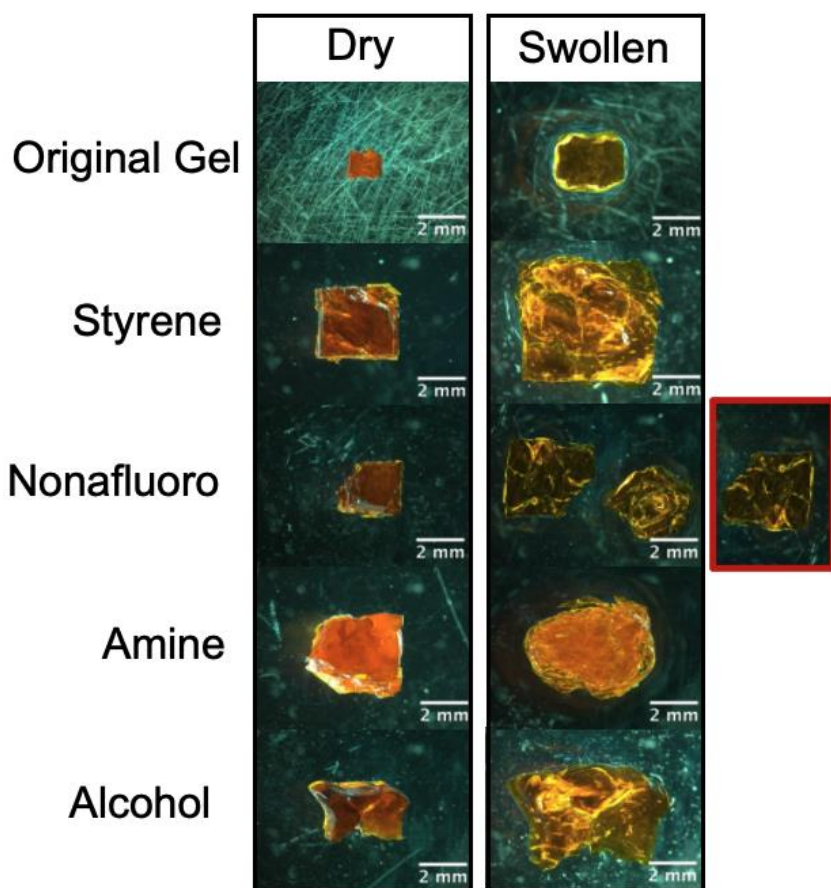

Figure 7. Images of the dry (left) and swollen (right) gels. These images were used to analyze the change in surface area and volume where applicable. All images were used as shown, except for the nonafluoro sample, which broke in its Z-axis. The portion outlined in red was used for calculations.

Table 1. Change in surface area of each azobenzene gel from swollen in DCM to dried out. These values were used to compare each gel to the unmodified, original gel system. (All Gels formed in DCM). Change is calculated by dividing the area of the swollen sample by that of the dried material.

Swollen-Dry Gel	Change in Area (%)	Compared to Allyloxy (%)
Original Gel	413.81	100.00
Styrene	283.31	68.46
Nonafluoro-1-hexene	196.00	47.36
Allylamine	153.65	37.13
Allyl Alcohol	275.61	66.60

Each gel underwent solvent exchanges into various solvents to test the effect of functionality on selectivity and conduct the actuation tests described in section 2.2.5. There are some notable differences in solvent preferences among the distinctive species when comparing the effects individually due to functional group interactions (Table S2). These are easily notable in Figure S11 which provides a visual comparison of the surface area changes of the individual gels compared to themselves in DCM. In this representation, all gels swell efficiently in DCM; however, THF is the second most efficient in the original, styrene, and alcohol gels, while it is the least in the amine and induces slightly higher swelling in the nonafluoro sample. The alcohol gel prefers acetone over toluene, unlike the other four, which have the 3rd most extensive swelling in toluene. In styrene, acetone is roughly 50% of the swelling observed in DCM. While the original gel swells decently in gasoline (75%), it does not absorb diesel as well (38%). These two solutions interact similarly in the functional materials, with the most significant difference in swelling observed in the styrene gel (9%). For both the styrene and alcohol gels, the swelling efficiency in gas, diesel, water, and hexafluorobenzene was below 50%. This suggests they would not be ideal at soaking up these materials, but it shows potential for selectively pulling the other solvents out of mixtures containing these (i.e., THF and water). The nonafluoro gel only swelled to 44%, its smallest size, in water and slightly preferred 1,1,1-trichlorotrifluoroethane (CFC), a perfluoro reagent. The allylamine had a minimum swelling of 63% in THF and exhibited a minimal variation in swelling (9% range) for all other non-DCM solvents.

The reason for the slight variation in the amine gel becomes apparent when the gels are compared to the maximum swelling in DCM. Table S3 shows the relative swelling percentages of each gel as a percentage compared to the maximum (original, DCM) derived from the data previously shown in Table 1. When this is extrapolated into a graph (Figure 8), the slight change in swelling in the amine gel is due to its overall low loading with a 45% maximum and total range of 16% change in surface area across all solvents. This data analysis shows alcohol's preference for acetone and THF compared to toluene, fuel, water, and a fluorocarbon ring. Alternatively, styrene functionalized gel absorbs acetone only slightly better than hexaflourobenzene (5.25%), most likely due to π-π interactions within the interstitial space. While a low absorption for fuels is less desirable, the low swelling in water is ideal, and styrene exhibits the lowest swelling in water of all gels at 27%. This provides insight into the selectivity for pollutants over water absorption, indicating the potential of these materials as remediation sponges that can be expanded and wrung out without physical interaction.
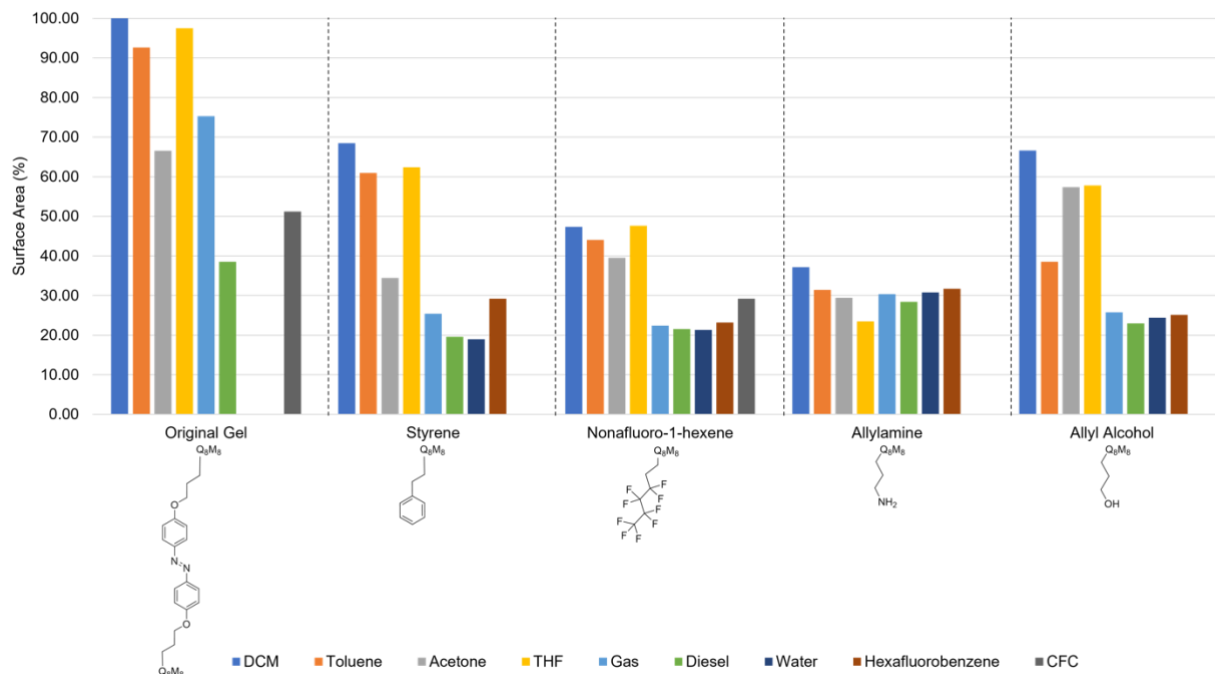
Figure 8. Initial, un-actuated surface areas of each gel in the given solvents, using the original gel's surface area in DCM as the reference maximum for all values. Graph derived from Table S3.

3.3. Photoactuation and Efficiency

As previously mentioned, DCM was found to swell the original material to its maximum and was used as the reference value for solvent and actuation effects. When conducting photo-actuation of the samples, an image was taken of the sample in the solvent (1), then after exposure to UV (365 nm, 30 min) and green light (515 nm, 30 min) in 3 cycles (1 hr each). An example of this process is shown in Figure S12. Measurements were derived from each image, and the change in surface area as a percentage of each gel was compiled in two ways like the swelling analysis, compared to itself (S) in DCM (Table S4) and against the original gel (O) in DCM (Table S5).

As discussed in Section 3.2, each functionalized gel demonstrates a distinct preference for swelling or absorbing certain solvents over others. The visual interpretation of the actuations of each material against themselves (Figure S13) and the original gel (Figure 9) offers a further understanding of each species' photodynamics in the various solvent systems. While there are many results to consider, we focus on any significant shrinking or expansion in surface area by actuation occurring from the 1st-3rd cycles to 565 nm green irradiation, and significant changes such as those exceeding a 5% variability. A decrease in surface area from the initial to the final state indicates a general loss of actuation potential. An overall increase indicates relaxation of the material structure and increased swelling potential. Any other unusual observations will be noted in detail below.
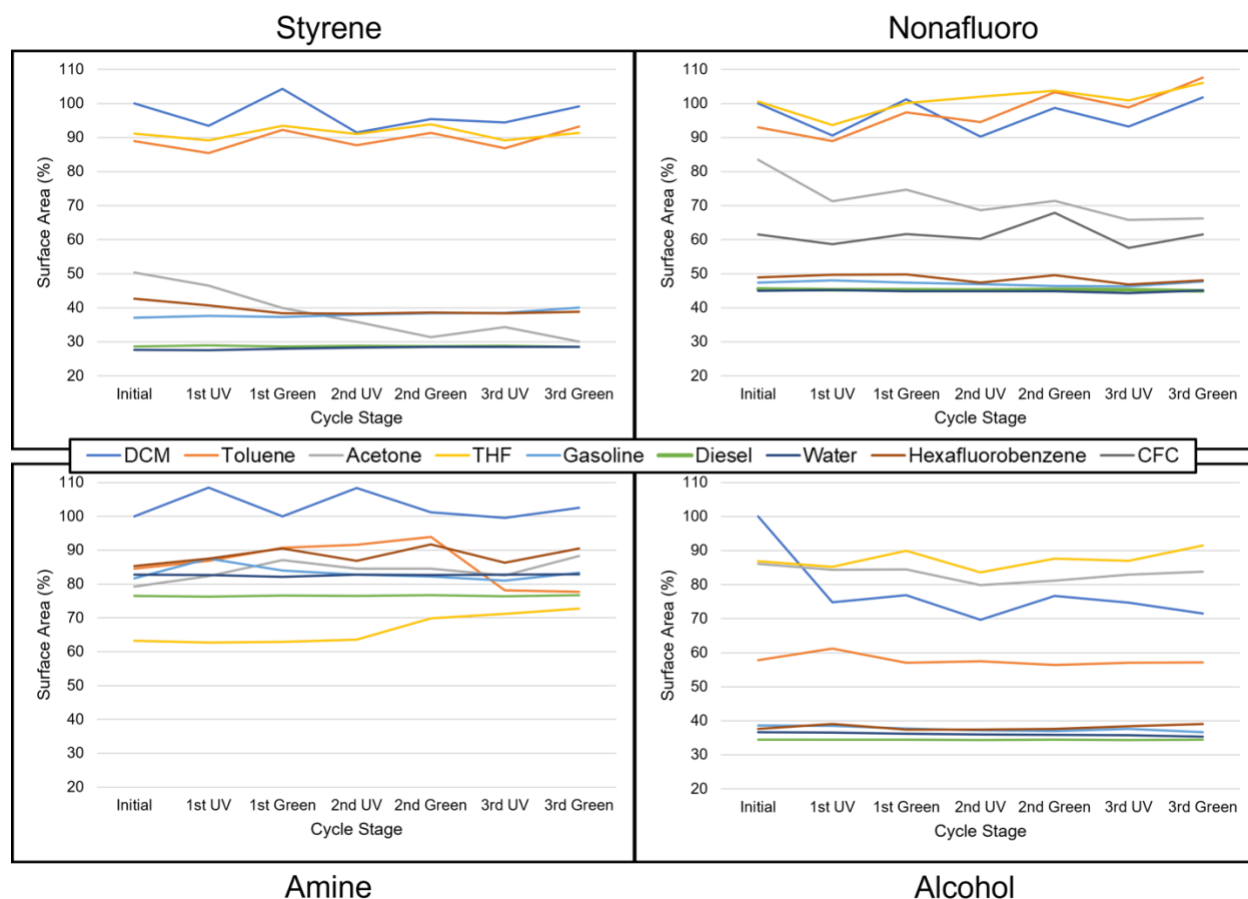

Figure 9. Graphs showing the actuation of each functionalized gel in the various solvents throughout three actuation cycles. Information depicts solvent swelling comparisons of each gel proportional to the original gel, where the data is derived from Table S3, and a range of 15-75% is shown.

The styrene functionalized networks were designed to decrease internal polarity vs. the original. It maintained the expected actuation response in DCM, relaxing in the first cycle before almost returning to its full size (compared to itself (S) 99.20%, and against the original gel (O) 67.91%). Toluene also showed great actuation and relaxation over each cycle, increasing from 88.98% → 93.24% (S) (60.92 → 63.84% O), showing a preference and expansion in similar, non-polar solvents with potential for π-π interactions. In contrast, the actuation in acetone was relatively

poor, reducing actuation from 50.34% $\rightarrow$ 30.09% (S), and 34.47% $\rightarrow$ 20.60% (O), which is likely due to its poor compatibility with this solvent. This is important as acetone is more polar than the other solvents and demonstrates our ability to alter the polarity of the pore/interstitial interiors. In these systems, the unfavorable solvents reduced the size of the gel and greatly halted the actuation of the material.

The nonafluoro functionalized network gel was expected to improve compatibility with fluorinated compounds. Overall, we see shrinkage and re-expansion over UV/Vis cycles (30 min each) for half of the solvents tested, with minimal changes occurring in gasoline, diesel, water, and hexafluorobenzene; however, there is some complexity in the quantification of the changes observed. DCM showed the most consistent results with reversible shrinkage and expansion changes of ~10% (S) or ~5% (O), slightly increasing capacity over 3 cycles from 100% $\rightarrow$ 101.78% (S) (47.36% $\rightarrow$ 48.21% O). Both Toluene and THF show improvement in swellability, where Toluene increases from 93.04% $\rightarrow$ 107.54% (S) (44.07% $\rightarrow$ 50.94% O) and THF from 100.60% $\rightarrow$ 106.00% (S) (47.65% $\rightarrow$ 50.21% O) showing a preference for these solvents over DCM. The material is less compatible with acetone, which shrinks from 83.47% $\rightarrow$ 66.26% (S) (39.54% $\rightarrow$ 31.3% O) steadily over the actuations. The compatibility of this perfluoro functionalized network with linear fluorinated solvents (CFC) is improved over the unmodified network when compared to its efficiencies (10.40%), but its photoresponse is not straightforward or overly consistent. The other solvents mostly lost their actuation capabilities, shrinking the material to under 50% (S) (30% O). There is speculation that the addition of the nonafluoro functional group and the ability of perfluoro substances to repel many substances results in reduced actuation.

Amine functionalized networks were designed to significantly increase the internal polarity versus the original, unfunctionalized material. This system was the most unique out of the derivatives, showing reverse UV and visible light performance, especially with DCM. UV exposure gave polymer expansion and green showed shrinkage of nearly 10% (S) in a contradictory fashion. There is no clear and consistent actuation with the other solvents. Acetone, toluene, THF, and hexafluorobenzene all saw changes of >5% (S), but when compared against the original gel, all solvents, except for DCM, swelled to less than 35%. The UV-Vis of the amine shows actuation and absorption similar to the original material; however, it is possible that the amine terminal groups interact with the azo bridge through hydrogen bonding to reduce or alter the expansion and contraction of the material.

The last functionalization investigated was alcohol, which was utilized to investigate the effects of increasing the internal polarity of the material, similar to the amine group. The first cycle of the alcohol in DCM showed an outstanding UV response, leading shrinkage to 74.77% (S) (66.60 $\rightarrow$ 49.80% O) of the original volume; however, additional cycles only gave up to 10% actuation response, ultimately remaining much smaller than it started 71.52% (S) (47.63% O). This hysteresis effect was sometimes observed in the unfunctionalized gel as well. The results in acetone and toluene tended to be quite inconsistent compared to the original; however, this material's affinity for acetone is the highest overall, even over the original material (+19.62%). This is potentially due to interactions between the -OH group and the acetone. In this sample, THF was the most consistent actuation and increased the overall material size from 86.83% $\rightarrow$71.52% (S) (57.83 $\rightarrow$60.93 O) after all three cycles.

These results show some selectivity for different solvents based on the functionality added within the material; however, all four variations have a low affinity for water, making them useful as pollutant sponges. Solvents or pollutants with low or no miscibility with water and high absorption, such as DCM or toluene, will cause the material to settle in the solvent layer above or below the water based on density (DCM – under, toluene on top). When dense solvents, like DCM, are expelled by "squeezing" the gel with UV, the pollutant will form bubbles or pockets around the material (Figure 10). When gels are exposed to a miscible solvent mixture, like THF, the material will selectively remove the solvent from the water, including any particulate dissolved in it. Figure S14 shows a demonstration of this, where a 1 M 9-fluorenone solution of 1-1 water-THF was dropped on the gel, and over a ~20-minute time frame with 515 nm light exposure, the dye-containing THF migrated towards and into the gel. The overall uptake of the functionalized materials is reduced compared to the original system, and incorporation of these groups may be slowing down actuation; however, the study described herein demonstrates the groundwork for future work on optimizing similar systems for specific uses and their ability to absorb and expel potential pollutants in aqueous environments selectively.
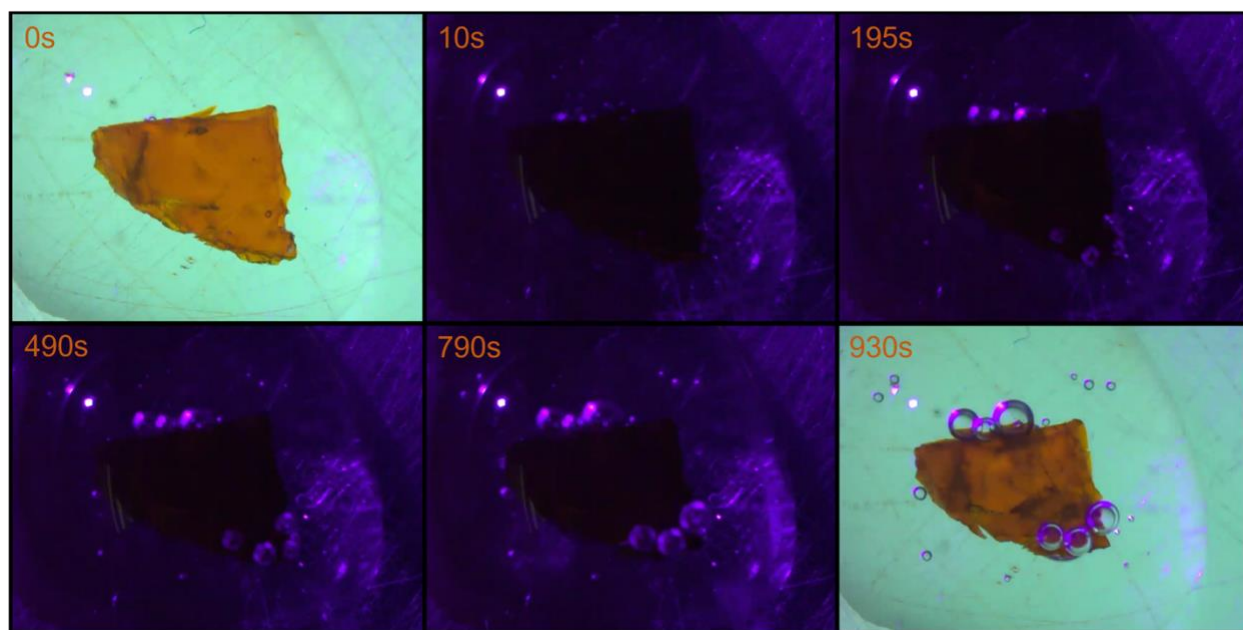

Figure 10. Still frame images of a DCM swelled styrene functionalized gel undergoing UV actuation "squeezing" while encapsulated in water (an incompatible solvent). After 930 seconds (15min, 30s), the DCM forms bubbles around the gel.

4. Conclusions

The work described above demonstrates the ability to use similar chemical moieties to purposefully target materials for removal. This study focused on the ability to affect the material's preference for swelling in various solvents and utilized a 1:2:4 mol ratio ($Q_8M_8^H$:azo:functional group) for this purpose. As demonstrated through the swelling and actuation of the gels and characterization, the functionalization of the original 4,4'-diallyloxy-azobenene – $Q_8M_8^H$ system affects the photo responsiveness, solvent preferability, and material properties.

A reduction in actuation potentials was observed (37-68%) compared to the original material, which suggests that the functional groups reduce the free space within the material, and future improvements may utilize lower loading levels or mixed functional groups to fine-tune the performance for specific processes. Two synthetic methods were utilized to generate the modified gels using a 1:2:4 mol ratio (Q_8:azo:functional group), but analysis by thermal gravimetric analysis and NMR indicates differences in the attachment efficiencies. Styrene and 3,3,4,4,5,5,6,6,6-nonafluoro-1-hexene were integrated as the system polymerized (in-situ), where the styrene indicates higher attachment based on the CY and NMR compared to the original material (90+%). Despite this, both materials exhibit distinct preferences for solvents and actuation efficiencies. It is suspected that incompatibilities of the fluorocarbon species caused it to disperse within the material unevenly, reducing its functionalization efficiency to ~60%. Interactions with the platinum catalyst (Karstedt's catalyst) required the integration of the amine and alcohol groups after the initial gelation process started. Attempts at synthesizing the materials in situ saw disruption of the polymerization process and halting gel formation. Injection of these groups into the material resulted in differences in material characteristics and behavior. While the alcohol group attached completely (100% by NMR and CY) and showed favorable actuation in some solvents, the amine materials swelled but saw little actuation. This is theorized to be the result of amine-platinum interactions reducing the efficiency of functionalization (65+%) and interactions of the bound amine groups with the N=N bond in the azobenzenes, altering the response to the wavelengths of light used as the electron density of these photoswitches increases.[26–30,33,60–62] While the amine gel did not perform as desired, the materials still swell, and this groups' known interactions with pharmaceuticals indicate a need for further optimization and understanding of this system. These findings provide grounds for improvement and insights for the selection of alternative functionalities with consideration for interactions with the solvent, catalyst, and photoswitch.

Notable changes in material solvent preference include selectivity for THF and fluorocarbons when 3,3,4,4,5,5,6,6,6-nonafluoro-hexene is incorporated into the gel, retaining a low absorption for water. This shows potential toward further investigation of these materials for fluorocarbon sequestration from waterways. The selectivity of styrene towards other aromatics and its low affinity for water absorption makes it a candidate for the removal of polycyclic aromatic hydrocarbons (PAH) and nanoplastics, specifically polystyrene, which presents a potential direction for future work. Choice of functionality shows potential for the selective removal of a variety of pollutants, and the gels can be designed to target specific contaminants based on polarity or structural interactions.

Conflicts of Interest

The authors declare no conflicts of interest with this article.

Author Contributions

Sims, C. B. conducted the bulk of the research, design, and writing of the manuscript. Chandler, E. T. synthesized starting materials and conducted gelation experiments and contributed to writing of the manuscript. Espitia Armenta, H. ran the TGA and proofread the manuscript. Hu, N-H. synthesized the original gel materials being compared and the first batches of azobenzene cross-

linkers. Furgal, J.C procured financial support, contributed to experimental design, and revised the manuscript.

Supporting Information

Figure S1 – mechanism of hydrosilylation; Figures S2-5 – UV-Vis of functionalized gels; Figure S6 – FTIR of gels; Figure S7 – TGA of gels; Table S1 – ceramic yields and calculations of gels,; Figure S8 – ^{13}C NMR of each gel; Figure S9 – Sem of functionalized gels; Figure S10 – Graphical swelling data; Figure S11 – graph of gel swelling in different solvents; Table S2 and S3 – Gel swelling; Figure S12 – example of gel actuations in DCM; Table S3 and S4 – surface area measurements of each gel individually and comparatively; Figure S13 – graph of individual gel actuations, Figure S14 – 9-fluorenone capture.

References

(1)   Gao, J.; Proulx, F.; Rodriguez, M. J. Occurrence and Spatio-Temporal Variability of Halogenated Acetaldehydes in Full-Scale Drinking Water Systems. *Sci. Total Environ.* **2019**, *693*, 133517.

(2)   Cordner, A.; De La Rosa, V. Y.; Schaider, L. A.; Rudel, R. A.; Richter, L.; Brown, P. Guideline Levels for PFOA and PFOS in Drinking Water: The Role of Scientific Uncertainty, Risk Assessment Decisions, and Social Factors. *J. Expo. Sci. Environ. Epidemiol.* **2019**, *29* (2), 157–171.

(3)   Wanner, P. Plastic in Agricultural Soils – A Global Risk for Groundwater Systems and Drinking Water Supplies? – A Review. *Chemosphere* **2021**, *264*, 128453.

(4)   Mudiyanselage, T. K.; Neckers, D. C. Highly Absorbing Superabsorbent Polymer. *J. Polym. Sci. A Polym. Chem.* **2008**, *46* (4), 1357–1364.

(5)   Lee, W.-F.; Hsu, C.-H. Superabsorbent Polymeric Material. V. Synthesis and Swelling Behavior of Sodium Acrylate and Sodium 2-Acrylamido-2-Methylpropanesulfonate Copolymeric Gels. *J. Appl. Polym. Sci.* **1998**, *69* (2), 229–237.

(6)   Okesola, B. O.; Smith, D. K. Applying Low-Molecular Weight Supramolecular Gelators in an Environmental Setting – Self-Assembled Gels as Smart Materials for Pollutant Removal. *Chem. Soc. Rev.* **2016**, *45* (15), 4226–4251.

(7)   Hu, N.; Lenora, C. U.; May, T. A.; Hershberger, N. C.; Furgal, J. C. In Situ Formed Methyl- Co - (Bis-R) Silsesquioxane Based Polymer Networks with Solvent Controlled Pore Size Distributions and High Surface Areas. *Mater. Chem. Front.* **2020**, *4,* 851-861.

(8)   Agrawal, A. K.; Das, M.; Jain, S. In Situ Gel Systems as 'Smart' Carriers for Sustained Ocular Drug Delivery. *Expert. Opin. Drug Deliv.* **2012**, *9* (4), 383–402.
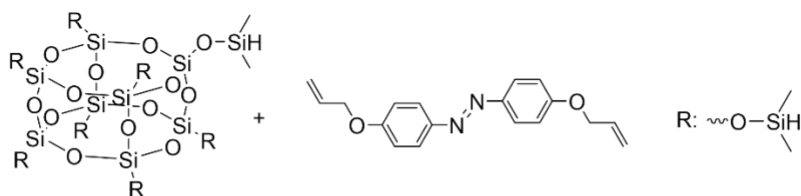
(9)   Matsumoto, A.; Tanaka, M.; Matsumoto, H.; Ochi, K.; Moro-oka, Y.; Kuwata, H.; Yamada, H.; Shirakawa, I.; Miyazawa, T.; Ishii, H.; Kataoka, K.; Ogawa, Y.; Miyahara, Y.; Suganami, T. Synthetic "Smart Gel" Provides Glucose-Responsive Insulin Delivery in Diabetic Mice. *Sci. Adv.* **2017**, *3* (11), eaaq0723.

(10)   Grove, T. Z.; Osuji, C. O.; Forster, J. D.; Dufresne, E. R.; Regan, L. Stimuli-Responsive Smart Gels Realized via Modular Protein Design. *J. Am. Chem. Soc.* **2010**, *132* (40), 14024–14026.

(11)   Chaterji, S.; Kwon, I. K.; Park, K. Smart Polymeric Gels: Redefining the Limits of Biomedical Devices. *Prog. Polym. Sci.* **2007**, *32* (8–9), 1083–1122.

(12)   Arndt, K.; Schmidt, T.; Richter, A.; Kuckling, D. High Response Smart Gels: Synthesis and Application. *Macromo.l Symp.* **2004**, *207* (1), 257–268.

(13)   Rodkate, N.; Rutnakornpituk, B.; Wichai, U.; Ross, G.; Rutnakornpituk, M. Smart Carboxymethylchitosan Hydrogels That Have Thermo- and PH-responsive Properties. *J. Appl. Polym. Sci.* **2015**, *132* (8), 41505.

(14)   Bag, D. S.; Saxena, A. K. Smart Gels. In *Kirk-Othmer Encyclopedia of Chemical Technology*; Wiley, 2014; pp 1–50.

(15)   Fan, F.; Wang, L.; Lu, X.; Liang, X.; Guo, Y. Synthesis and Application of Smart Gel Material Modified Silica Microspheres for PH-Responsive Hydrophilicity in Liquid Chromatography. *Analyst* **2021**, *146* (20), 6262–6269.

(16)   An, Z.; Zhang, J.-M.; Lv, M.-Y.; Li, X.-Q.; Wu, L.; Shang, H.-B.; Li, D. Light-Driven Polarity Switching of the Chromatographic Stationary Phase with Photoreversibility. *Anal. Chem.* **2021**, *93* (51), 17051–17059.

(17)   Jones, C. D.; Steed, J. W. Gels with Sense: Supramolecular Materials That Respond to Heat, Light and Sound. *Chem. Soc. Rev.* **2016**, *45* (23), 6546–6596.

(18)   Wojtecki, R. J.; Nelson, A. Small Changes with Big Effects: Tuning Polymer Properties with Supramolecular Interactions. *J. Polym. Sci. A Polym. Chem.* **2016**, *54* (4), 457–472.

(19)   Cashin, V. B.; Eldridge, D. S.; Yu, A.; Zhao, D. Surface Functionalization and Manipulation of Mesoporous Silica Adsorbents for Improved Removal of Pollutants: A Review. *Environ. Sci. (Camb)* **2018**, *4* (2), 110–128.

(20)   Wieszczycka, K.; Staszak, K.; Woźniak-Budych, M. J.; Litowczenko, J.; Maciejewska, B. M.; Jurga, S. Surface Functionalization – The Way for Advanced Applications of Smart Materials. *Coord. Chem. Rev.* **2021**, *436*, 213846.

(21)   Zhang, X.; Lu, Q.; Chen, C.; Li, X.; Qing, G.; Sun, T.; Liang, X. Smart Polymers Driven by Multiple and Tunable Hydrogen Bonds for Intact Phosphoprotein Enrichment. *Sci. Technol. Adv. Mater.* **2019**, *20* (1), 858–869.

(22)   Qing, G.; Lu, Q.; Li, X.; Liu, J.; Ye, M.; Liang, X.; Sun, T. Hydrogen Bond Based Smart Polymer for Highly Selective and Tunable Capture of Multiply Phosphorylated Peptides. *Nat. Commun.* **2017**, *8* (1), 461.

(23)   Barczak, M.; Dobrowolski, R.; Borowski, P.; Giannakoudakis, D. A. Pyridine-, Thiol- and Amine-Functionalized Mesoporous Silicas for Adsorptive Removal of Pharmaceuticals. *Micropor. Mesopor. Mat.* **2020**, *299*, 110132.

(24)   Gan, D.; Lyon, L. A. Tunable Swelling Kinetics in Core−Shell Hydrogel Nanoparticles. *J Am Chem. Soc.* **2001**, *123* (31), 7511–7517.

(25)   Barrett, C. J.; Mamiya, J.; Yager, K. G.; Ikeda, T. Photo-Mechanical Effects in Azobenzene-Containing Soft Materials. *Soft Matter.* **2007**, *3* (10), 1249.

(26)   Beharry, A. A.; Sadovski, O.; Woolley, G. A. Azobenzene Photoswitching without Ultraviolet Light. *J. Am. Chem. Soc.* **2011**, *133* (49), 19684–19687.

(27) Dong, M.; Babalhavaeji, A.; Samanta, S.; Beharry, A. A.; Woolley, G. A. Red-Shifting Azobenzene Photoswitches for in Vivo Use. *Acc. Chem. Res.* **2015**, *48* (10), 2662–2670.

(28) Kerckhoffs, A.; Christensen, K. E.; Langton, M. J. Fast Relaxing Red and Near-IR Switchable Azobenzenes with Chalcogen and Halogen Substituents: Periodic Trends, Tuneable Thermal Half-Lives and Chalcogen Bonding. *Chem. Sci.* **2022**, *13* (39), 11551–11559.

(29) Bléger, D.; Schwarz, J.; Brouwer, A. M.; Hecht, S. O -Fluoroazobenzenes as Readily Synthesized Photoswitches Offering Nearly Quantitative Two-Way Isomerization with Visible Light. *J. Am. Chem. Soc.* **2012**, *134* (51), 20597–20600.

(30) Mehrparvar, S.; Scheller, Z. N.; Wölper, C.; Haberhauer, G. Design of Azobenzene beyond Simple On–Off Behavior. *J Am Chem Soc* **2021**, *143* (47), 19856–19864.

(31) Younis, M.; Ahmad, S.; Atiq, A.; Amjad Farooq, M.; Huang, M.; Abbas, M. Recent Progress in Azobenzene-Based Supramolecular Materials and Applications. *The Chemical Record* **2023**, *23* (11), e202300126.

(32) Mahimwalla, Z.; Yager, K. G.; Mamiya, J.; Shishido, A.; Priimagi, A.; Barrett, C. J. Azobenzene Photomechanics: Prospects and Potential Applications. *Polymer Bulletin* **2012**, *69* (8), 967–1006.

(33) Bandara, H. M. D.; Burdette, S. C. Photoisomerization in Different Classes of Azobenzene. *Chem. Soc. Rev.* **2012**, *41* (5), 1809–1825.

(34) Kumar, G. S.; Neckers, D. C. Photochemistry of Azobenzene-Containing Polymers. *Chem. Rev.* **1989**, *89* (8), 1915–1925.

(35) Oscurato, S. L.; Salvatore, M.; Maddalena, P.; Ambrosio, A. From Nanoscopic to Macroscopic Photo-Driven Motion in Azobenzene-Containing Materials. *Nanophotonics* **2018**, *7* (8), 1387–1422.

(36) Galante, M. J.; Zucchi, I. A.; Oyanguren, P. A.; Sáiz, L. M. Light-Induced Healing in Azobenzene Bridged Silsesquioxanes. *Eur. Polym. J.* **2019**, *117*, 382–390.

(37) Yesodha, S. K.; Sadashiva Pillai, C. K.; Tsutsumi, N. Stable Polymeric Materials for Nonlinear Optics: A Review Based on Azobenzene Systems. *Prog. Polym. Sci.* **2004**, *29* (1), 45–74.

(38) Dong, L.; Feng, Y.; Wang, L.; Feng, W. Azobenzene-Based Solar Thermal Fuels: Design, Properties, and Applications. *Chem. Soc. Rev.* **2018**, *47* (19), 7339–7368.

(39) Xu, G.; Li, S.; Liu, C.; Wu, S. Photoswitchable Adhesives Using Azobenzene-Containing Materials. *Chem. Asian. J.* **2020**, *15* (5), 547–554.

(40) Chen, Y.; Fang, Y.; Yu, J.; Gao, W.; Zhao, H.; Zhang, X. A Silsesquioxane-Porphyrin-Based Porous Organic Polymer as a Highly Efficient and Recyclable Absorbent for Wastewater Treatment. *J. Hazard. Mater.* **2021**, *406*, 124769.

(41) Weis, P.; Wu, S. Light-Switchable Azobenzene-Containing Macromolecules: From UV to Near Infrared. *Macromol. Rapid Commun.* **2018**, *39* (1), 1–12.

(42) Kakuta, T.; Takashima, Y.; Nakahata, M.; Otsubo, M.; Yamaguchi, H.; Harada, A. Preorganized Hydrogel: Self-Healing Properties of Supramolecular Hydrogels Formed by Polymerization of Host–Guest-Monomers That Contain Cyclodextrins and Hydrophobic Guest Groups. *Adv. Mater.* **2013**, *25* (20), 2849–2853.

(43) Takashima, Y.; Hatanaka, S.; Otsubo, M.; Nakahata, M.; Kakuta, T.; Hashidzume, A.; Yamaguchi, H.; Harada, A. Expansion–Contraction of Photoresponsive Artificial Muscle Regulated by Host–Guest Interactions. *Nat. Commun.* **2012**, *3* (1), 1270.

(44) Pan, Z.; Liu, M.; Zheng, C.; Gao, D.; Huang, W. Study of Karstedt's Catalyst for Hydrosilylation of a Wide Variety of Functionalized Alkenes with Triethoxysilane and Trimethoxysilane. *Chin J Chem* **2017**, *35* (8), 1227–1230. https://doi.org/10.1002/cjoc.201700024.
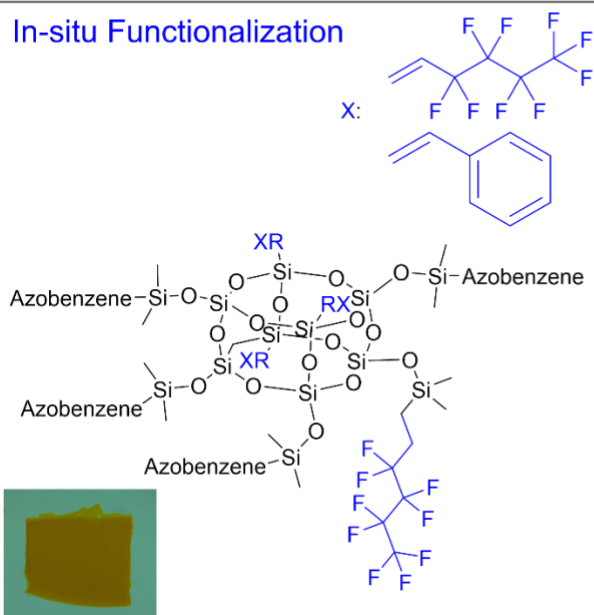
(45)   Romero, G.; Wang, X. *Hydrosilylation*. LibreTexts Chemistry. https://chem.libretexts.org/Bookshelves/Inorganic_Chemistry/Supplemental_Modules_and_Web sites_(Inorganic_Chemistry)/Catalysis/Catalyst_Examples/Hydrosilylation.

(46)   Nakajima, Y.; Shimada, S. Hydrosilylation Reaction of Olefins: Recent Advances and Perspectives. *RSC Adv.* **2015**, *5* (26), 20603–20616.

(47)   P. D'Amelia, R.; Mancuso, J.; F. Nirode, W.; Singh, S. Characterization and Synthesis of Functionalized Polysilalkylene Siloxane Monomers by Hydrosilylation Reaction. *World Journal of Organic Chemistry* **2019**, *7* (1), 5–13. https://doi.org/10.12691/wjoc-7-1-2.

(48)   Liao, J.; Wang, W.; Xu, X.; Jian, H.; Yang, S. Interfacial Behavior of Giant Amphiphiles Composed of Azobenzene and Polyhedral Oligomeric Silsesquioxane. *Langmuir* **2022**, *38* (4), 1611–1620.

(49)   Ledin, P. A.; Tkachenko, I. M.; Xu, W.; Choi, I.; Shevchenko, V. V.; Tsukruk, V. V. Star-Shaped Molecules with Polyhedral Oligomeric Silsesquioxane Core and Azobenzene Dye Arms. *Langmuir* **2014**, *30* (29), 8856–8865.

(50)   Zhou, J.; Zhao, Y.; Yu, K.; Zhou, X.; Xie, X. Synthesis, Thermal Stability and Photoresponsive Behaviors of Azobenzene-Tethered Polyhedral Oligomeric Silsesquioxanes. *New J. Chem.* **2011**, *35* (12), 2781. https://doi.org/10.1039/c1nj20577c.

(51)   Liu, Y.; Yang, W.; Liu, H. Azobenzene-Functionalized Cage Silsesquioxanes as Inorganic–Organic Hybrid, Photoresponsive, Nanoscale, Building Blocks. *Chem. Eur. J.* **2015**, *21* (12), 4731–4738.

(52)   Dudziec, B.; Żak, P.; Marciniec, B. Synthetic Routes to Silsesquioxane-Based Systems as Photoactive Materials and Their Precursors. *Polymers.* **2019**, *11* (3), 504.

(53)   Liu, N.; Yu, K.; Smarsly, B.; Dunphy, D. R.; Jiang, Y.-B.; Brinker, C. J. Self-Directed Assembly of Photoactive Hybrid Silicates Derived from an Azobenzene-Bridged Silsesquioxane. *J. Am. Chem. Soc.* **2002**, *124* (49), 14540–14541.

(54)   Tkachenko, I. M.; Kobzar, Y. L.; Korolovych, V. F.; Stryutsky, A. V.; Matkovska, L. K.; Shevchenko, V. V.; Tsukruk, V. V. Novel Branched Nanostructures Based on Polyhedral Oligomeric Silsesquioxanes and Azobenzene Dyes Containing Different Spacers and Isolation Groups. *J. Mater. Chem. C.* **2018**, *6* (15), 4065–4076.

(55)   Guo, S.; Okubo, T.; Kuroda, K.; Shimojima, A. A Photoresponsive Azobenzene-Bridged Cubic Silsesquioxane Network. *J. Solgel. Sci. Technol.* **2016**, *79* (2), 262–269.

(56)   Hu, N.; Furgal, J. C. Photoreversible Loading and Unloading of Q–Silsesquioxane Dynamic Network Sponges. *Adv. Funct. Mater.* **2021**, *31* (13), 1–11.

(57)   Zhang, C.; Laine, R. M. Hydrosilylation of Allyl Alcohol with $[HSiMe_2OSiO_{1.5}]_8$:Octa(3-Hydroxypropyldimethylsiloxy)Octasilsesquioxane and Its Octamethacrylate Derivative as Potential Precursors to Hybrid Nanocomposites. *J. Am. Chem. Soc.* **2000**, *122* (29), 6979–6988.

(58)   Knight, C. T. G.; Kirkpatrick, R. J.; Oldfield, E. The Connectivity of Silicon Sites in Silicate Glasses, as Determined by Two-dimensional [29]Si Nuclear Magnetic Resonance Spectroscopy. *J. Non Cryst. Solids* **1990**, *116*, 140–144.

(59)   Uhlig, F.; Marsmann, H. C. *^{29}Si NMR Some Practical Aspects*. https://www.pascal-man.com/periodic-table/29Si.pdf (accessed 2024-05-07).

(60)   Yager, K. G.; Barrett, C. J. Novel Photo-Switching Using Azobenzene Functional Materials. *J Photochem. Photobiol. A Chem.* **2006**, *182* (3), 250–261.

(61)   Crecca, C. R.; Roitberg, A. E. Theoretical Study of the Isomerization Mechanism of Azobenzene and Disubstituted Azobenzene Derivatives. *J. Phys. Chem. A* **2006**, *110* (26), 8188–8203.

(62) Ishikawa, T.; Noro, T.; Shoda, T. Theoretical Study on the Photoisomerization of Azobenzene. *J. Chem. Phys.* **2001**, *115* (16), 7503–7512.

Table of Contents Image